Journal of Solid State Chemistry 300 (2021) 122241

Contents lists available at ScienceDirect

Journal of Solid State Chemistry

journal homepage: www.elsevier.com/locate/jssc

The phase evolution of tetradymite-type bismuth selenide in alkali ion batteries

Conrad Gillard [a], Kathleen Djohari [a], Partha Pratim Jana [b], Maxim Avdeev [c,d], Neeraj Sharma [a,*]

[a] University of New South Wales, Sydney, NSW, 2052, Australia
[b] Department of Chemistry, Indian Institute of Technology, Kharagpur, West Bengal, 721302, India
[c] Australian Nuclear Science and Technology Organisation, Kirrawee DC, NSW, 2232, Australia
[d] School of Chemistry, The University of Sydney, Sydney, NSW, 2006, Australia

ARTICLE INFO

Keywords:
Layered metal chalcogenides
Ex-situ X-ray diffraction
Phase evolution
Lithium ion batteries
Sodium ion batteries
Potassium ion batteries

ABSTRACT

Tetradymite-type Bi_2Se_3 is synthesised via a solid-state method, and its phase evolution in Li, Na and K half-cells is experimentally investigated. Ex-situ X-ray diffraction data is analysed with the Rietveld method, indicating intercalation, conversion and alloying reactions for all systems. Direct evidence of alloying is observed in the cases of the Li and Na systems while alloying is inferred for the K system. In addition, a preliminary study of the performance of Bi_2Se_3 as an electrode material for rechargeable Li, Na and K-half cells is undertaken. High initial capacities of 560, 680 and 1000 mAh/g for Li, Na and K respectively are observed. However, capacity fade is severe in all cases, with 10^{th} cycle capacity decreases of 68%, 79% and 90% respectively. This poor cyclability is likely attributable to the large volume changes that accompany the conversion and alloying reactions. Finally, the magnetic properties of the resultant intercalated materials are investigated. Li intercalation induces a divergence between zero-field cooled and field cooled curves below 150 K, whereas Na and K intercalation do not have significant effects on the observed magnetic properties.

1. Introduction

Tetradymite-type Bi_2Se_3 has been the subject of academic and industrial research for several decades, initially due to its intriguing thermoelectric properties [1]. In recent years, Bi_2Se_3 has been found to possess additional exotic properties such as topological insulativity [2] and proximity induced superconductivity [3]. Consequently, techniques to modify the structure of Bi_2Se_3 are highly prospective, as they may enhance these properties. The tetradymite-type crystal structure adopts the hexagonal space group $R\bar{3}m$ (space group number 166) and possesses a unit cell consisting of layers that are arranged in the sequence: Ch-M-Ch-M-Ch, in which Ch denotes a chalcogenide and M a metal. These quintuple layers are in turn stacked along the *c* crystallographic axis and are separated by Van der Waals gaps [4]. The relatively weak nature of the out of plane (or layer) Van der Waals interactions is responsible for the capability of tetradymite type materials to host alkali metal ion intercalants [5–7] and allow facile alkali ion diffusivity [8–10]. Tetradymite-type materials typically exhibit moderate electrical conductivity. For instance, the precise room temperature electrical conductivity of Bi_2Se_3 varies between samples, however 400 S cm^{-1} represents a typical value [11].

These properties have rendered tetradymites prospective as alkali ion battery negative electrode materials, and several investigations into this application have been published [7–10,12–14]. High first discharge capacities were consistently reported, due to the capability of tetradymites to accommodate 12 alkali metal ions per formula unit, via conversion and alloying reactions [7–10,14]. The general formulae of these reactions are shown in Equations (1) and (2) respectively, in which M, Ch and X denote a metal, a chalcogen and an alkali metal, respectively.

$$M_2Ch_3 + 6X \rightarrow 3X_2Ch + 2\,M \quad (1)$$

$$2\,M + 6X \rightarrow 2MX_3 \quad (2)$$

Poor cyclability was consistently reported, attributable to volume changes associated with the above reactions [7–10]. However cycle life was significantly improved with blending and nanosizing techniques [12–14].

The phase evolution and cyclability of Bi_2Se_3 in Li half cells was investigated by Ali et al., who synthesised two nanosized forms and compared their performance [15]. The reported electrochemical performance was largely consistent with the wider literature on tetradymite

* Corresponding author.
E-mail address: neeraj.sharma@unsw.edu.au (N. Sharma).

https://doi.org/10.1016/j.jssc.2021.122241
Received 27 March 2021; Received in revised form 26 April 2021; Accepted 27 April 2021
Available online 1 May 2021

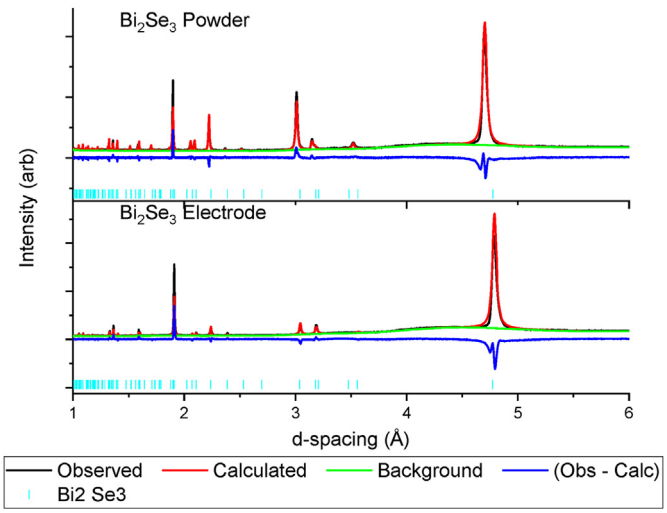

Fig. 1. Rietveld refinement of the Bi_2Se_3 structural model with PXRD data of as-received Bi_2Se_3 powder before and after electrode casting.

Table 1
Rietveld refined model parameters of as-received Bi_2Se_3 powder and processed electrode.

Sample	Bi_2Se_3 *a*	Bi_2Se_3 *c*	w*R*
Powder	4.1434(3)	28.6483(9)	8.14%
Electrode	4.1395(7)	28.634(1)	13.22%

electrodes, with high first discharge capacities and rapid cycle fade. However, the proposed phase evolution sequence differed slightly, as the authors identified only intercalation and conversion type reactions, and did not include an alloying reaction in their scheme. We speculate that the source of this discrepancy may be that the reactions were identified on the basis of the discharge profiles rather than structural studies, e.g. via X-ray diffraction, of the discharged electrodes. Additionally, the electrochemical performance and phase evolution of Bi_2Se_3 versus Na and K half cells have not yet been investigated.

Intercalation-induced property modification of Bi_2Se_3 (or a doped variant thereof) was investigated by two recent studies, with intriguing results. Firstly, the intercalation of 0.12 Cu atoms per Bi_2Se_3 formula unit induced superconductivity, with a critical temperature of 3.8 K [16]. Secondly, the electrochemical intercalation of Li within $Bi_2Se_{0.3}Te_{2.7}$ enhanced the thermoelectric properties [12]. However, property modification of undoped Bi_2Se_3 via electrochemical intercalation of alkali metals has not yet been investigated. This is despite the publication of several studies reporting the occurrence of Li intercalation within Bi_2Se_3 (or doped variants thereof) during discharge of Li half-cells [6,15,17–20]. It should also be noted that numerous publications report intercalation-induced property modification of non-tetradymite layered metal chalcogenides, and several excellent reviews summarise these [21,22].

Based on the preceding analysis, several knowledge gaps were identified. Firstly, understanding of the phase evolution of the Bi_2Se_3 versus Li system appears incomplete, due to uncertainty relating to the occurrence of an alloying reaction. Secondly, the performance and phase evolution of Bi_2Se_3 versus Na and K half cells have not been investigated, presenting intriguing avenues of inquiry. Finally, the properties of alkali

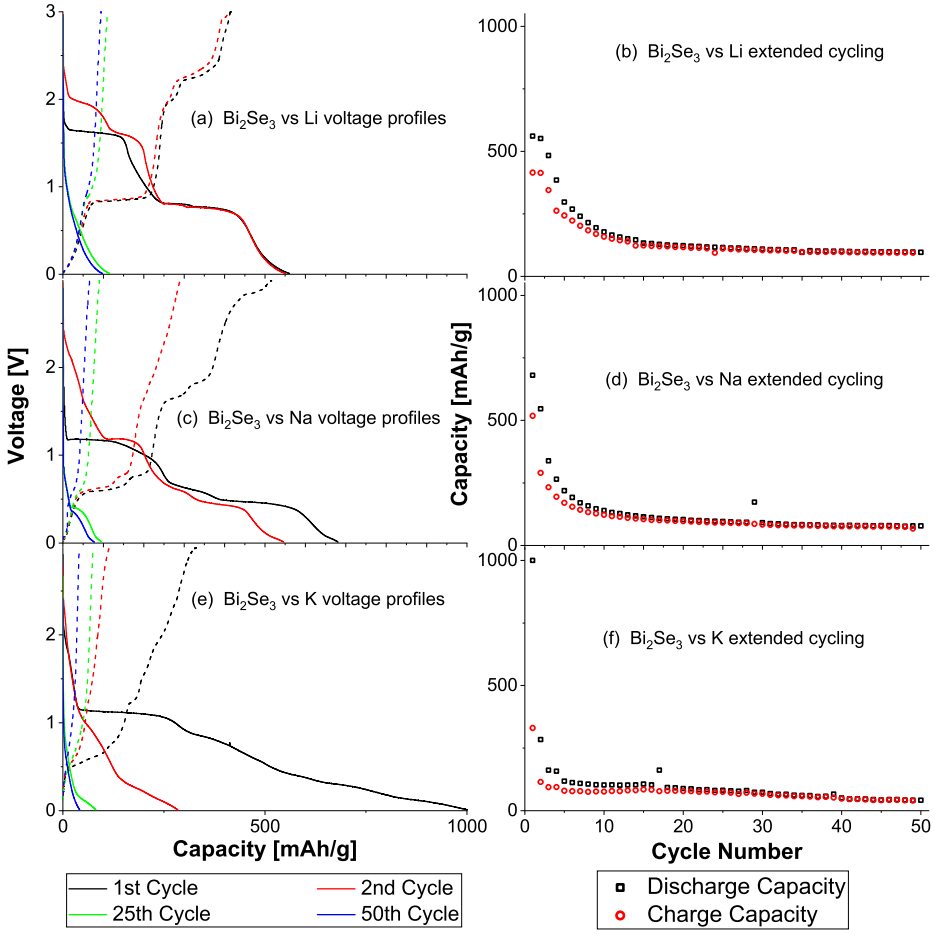

Fig. 2. Selected discharge-charge and extended cycling curves for Bi_2Se_3 versus Li(a,b) Na(c,d) and K(e,f) half cells.

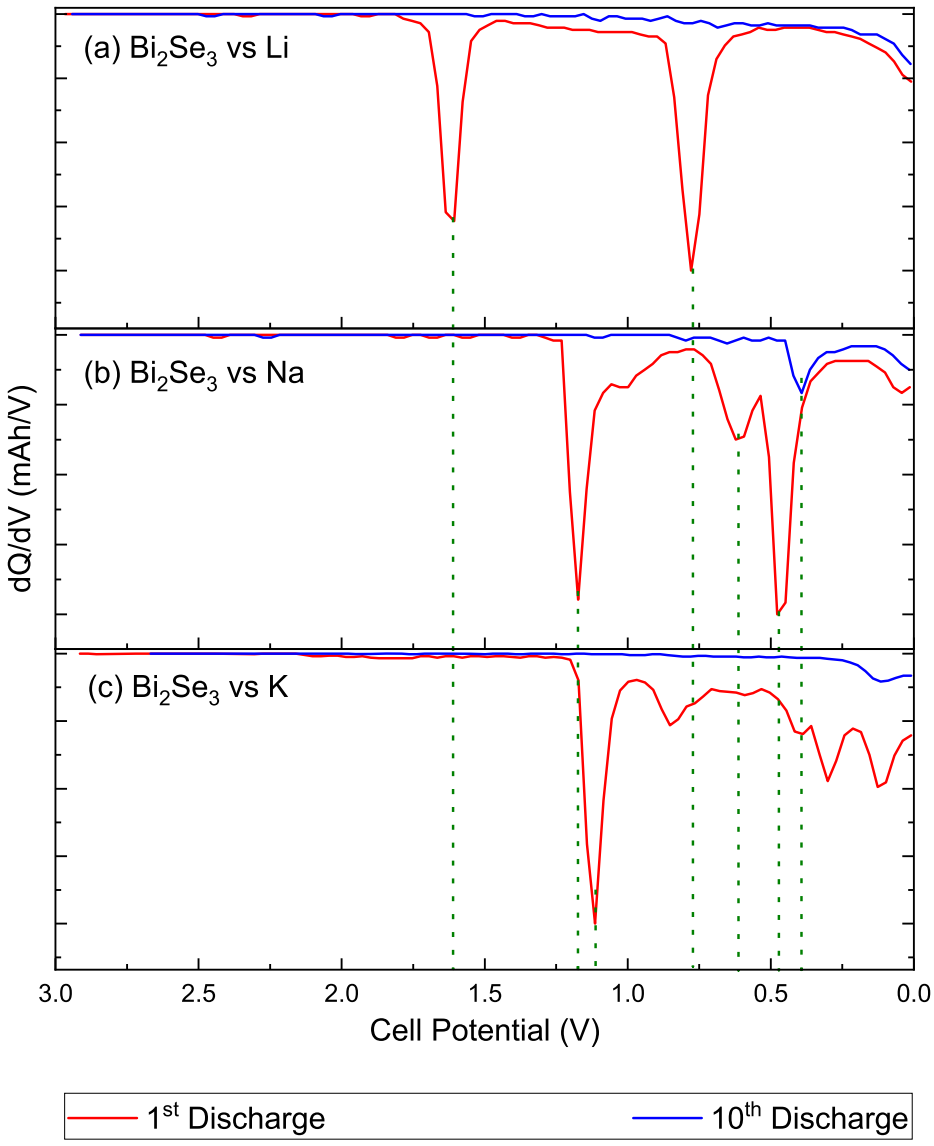

Fig. 3. Differential discharge capacity versus voltage plots for Bi_2Se_3 versus Li(a), Na(b) and K(c) half cells. Droplines indicate the voltages at which features occur.

metal-intercalated Bi_2Se_3 have not yet been measured, despite several studies demonstrating that this may be accomplished electrochemically.

In order to address these knowledge gaps, in this study Bi_2Se_3 was synthesised by a solid-state method and was used to construct lithium, sodium and potassium ion half-cells. Extended cycling experiments were performed, and discharge profiles and differential capacity plots were formulated. The phase evolution of each system was then investigated using ex-situ powder X-ray diffraction (PXRD) in conjunction with the electrochemical measurements. Finally, a preliminary investigation into intercalation-induced property modifications was performed by measuring the magnetic properties of the resultant intercalated materials.

2. Materials and methods

Bi_2Se_3 was synthesised via a high temperature solid state method using highly pure Bi (Powder, 200 mesh, 99.999% Alfa Aesar) and Se (Shot, 2–6 mm, 99.999% Alfa Aesar). Elements were precisely weighed and loaded inside an argon atmosphere glove box and sealed in silica ampoules. The ampoules were heated to 993 K at a rate of 5 K/min and held at this temperature for 96 h. The furnace was then switched off and the samples were allowed to cool to room temperature (RT).

Slurries were formulated by mixing ground Bi_2Se_3 with carbon black and polyvinylidene fluoride in a 8 : 1: 1 ratio. N-methyl-2-pyrrolidone solvent was added in a quantity sufficient to make a thick slurry, and the mixture was stirred in an argon atmosphere glovebox for 24 h. Subsequently, the slurry was cast onto a copper foil, using a doctor blade. Lithium, sodium and potassium metal half-cells were constructed using the resultant electrode sheets, following standard literature methods [23]. Stainless steel CR2032 coin cell cases, wave springs and spacers were all purchased from MTI. For the case of lithium half cells, 1 M $LiPF_6$ dissolved in an equivolumetric mixture of ethylene carbonate (EC) and dimethyl carbonate (DMC) and was used as the electrolyte. For the cases of sodium and potassium metal half cells respectively, 1 M $NaPF_6$ and 0.8 M KPF_6 in EC/DMC were used as electrolytes. Following construction, each battery was rested for 24 h then either discharged galvanostatically or cycled, at a current density of 15 mA/g using a Neware battery cycler. For the case of ex-situ experiments, the batteries were discharged to a targeted capacity, after which they were immediately transferred to an argon atmosphere glovebox and disassembled. The extracted electrodes were washed with dimethyl carbonate in order to remove any electrolyte solution and salts adhered to the surface. They were then left for 24–48 h to allow any residual DMC to evaporate.

Powder X-ray diffraction (PXRD) was used to investigate the structural evolution of the Bi_2Se_3 electrodes. Diffraction patterns were

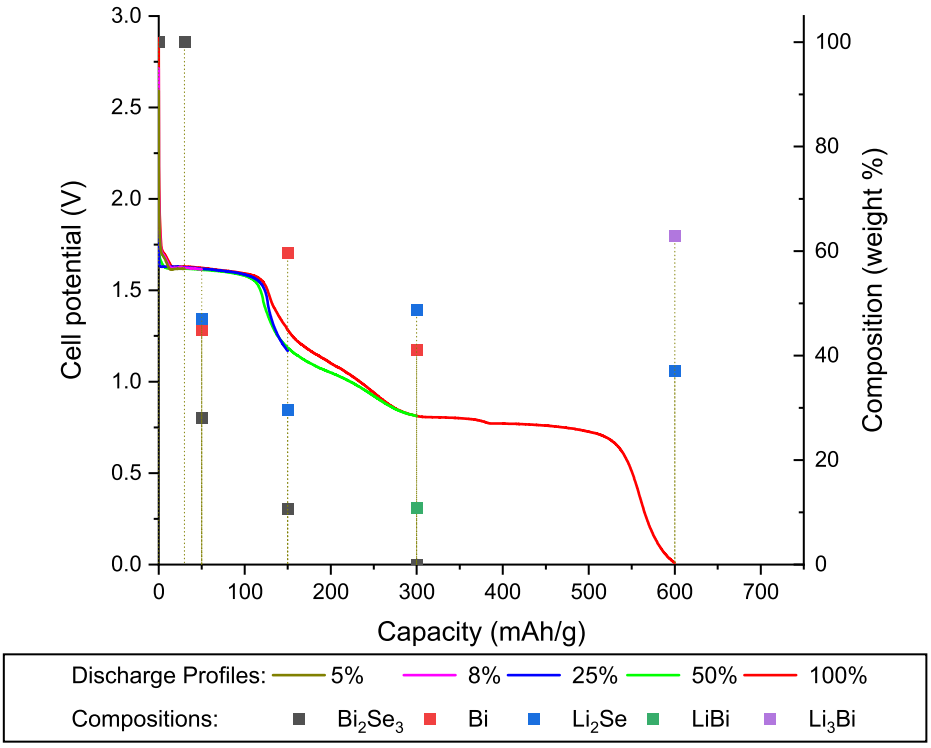

Fig. 4. Discharge profiles and weight fractions of Bi_2Se_3 versus Li ex-situ experiments.

collected using a Panalytical Aeris Benchtop laboratory X-ray diffractometer, utilising Cu source radiation. Samples were prepared by scraping the electrode material off the current collector and transferring to an air-tight sample holder. The sample was not ground, and the sample holder was sealed before removing from the argon filled glovebox. The Rietveld method was used to refine structural models with the PXRD data, using the General Structural Analysis System-II (GSAS-II) software package [24].

A Quantum Design EverCool-II 9T physical properties measurement system with vibrating sample magnetometry option was used to measure magnetic susceptibility data from the powder samples. Temperature dependent magnetic susceptibility data was collected under zero field cooled (ZFC) and field cooled (FC) conditions upon warming from 3 to 300 K, with an applied field of 1000 Oe.

3. Results and discussion

3.1. Structural evolution during electrode processing

Rietveld refinements of the Bi_2Se_3 structural model using PXRD data collected from an Bi_2Se_3 electrode disc (after processing) and from the as-prepared powder were performed, as shown in Fig. 1. Lattice parameters, instrument parameters and preferred orientation were refined for each sample, and the atomic parameters were left fixed at their initial values. In order to maintain consistency, the same set of parameters were refined for all Rietveld analyses in this work. A background feature is observed in all PXRD data in this work and is attributable to a Kapton foil used to protect the samples from air contact. Intensities and peak shapes exhibited close agreement in both samples. Slight shifts in peak positions were observed, corresponding to slight contractions in the *a* and *c* lattice parameters in the electrode sample relative to the powder, as shown in Table 1. Additionally, the intensity of the (1,0,-5) and (1,0,10) decreased in the electrode sample, likely due to preferred orientation caused by the casting process. The similarity of the lattice parameters between samples indicated that only minor structural changes occurred during processing.

3.2. Electrochemical performance

Li, Na and K half cells were cycled, and the resultant charge-discharge profiles and capacity versus cycle number plots are presented in Fig. 2. High first discharge capacities of 560, 680 and 1000 mAh/g were exhibited by the Li, Na and K half cells respectively. Assuming the transfer of 12 alkali ions per formula unit, the theoretical capacity of each system was 491 mAh/g. Consequently, the initial capacities exceeded the theoretical value, which is suggestive of electrolyte-electrode reactions. In all cases rapid capacity fades were observed, with 10^{th} cycle capacity decreases of 68%, 79% and 90% for the Li, Na and K systems respectively. Similar trends were reported by previous studies on the electrochemical performance of Bi_2Se_3 and other TTLMCs [7–10]. The inverse proportionality between capacity and alkali atomic mass in the first discharge contrasted with the case of graphite, which exhibited the following trend: Li > K > Na [25]. However, it should be noted that graphite forms intercalation compounds with these alkali ions, whereas Bi_2Se_3 undergoes intercalation, conversion and alloying reactions. Therefore, it is likely that the extent to which these reactions approached completion, and/or the degree to which electrode-electrolyte reactions occurred, are responsible for the observed capacities. It should also be noted that the capacity of the K system rapidly decreased after the first cycle (see Fig. 2) suggesting poorer reversibility than the Li and Na systems.

The voltage window of all systems was primarily within the 0–3 V range, which suggested a possible application as an alkali ion battery negative electrode material. The commercial viability of this prospect was briefly assessed by comparing the performance and price of Bi_2Se_3 to graphite, which is considered the benchmark anode material for lithium-ion batteries. Based on prices from Sigma Aldrich for research quantities of these materials, the cost of Bi_2Se_3 exceeded that of battery grade graphite by a factor of 64 [26,27]. Regarding performance, 100^{th} cycle discharge capacities of 250, 200 and 210 mAh/g have been reported for Li, Na and K ion batteries respectively, with graphite or expanded graphite anodes [28–30]. These significantly exceeded the 50^{th} cycle discharge capacities for Bi_2Se_3 obtained from our experiments, which

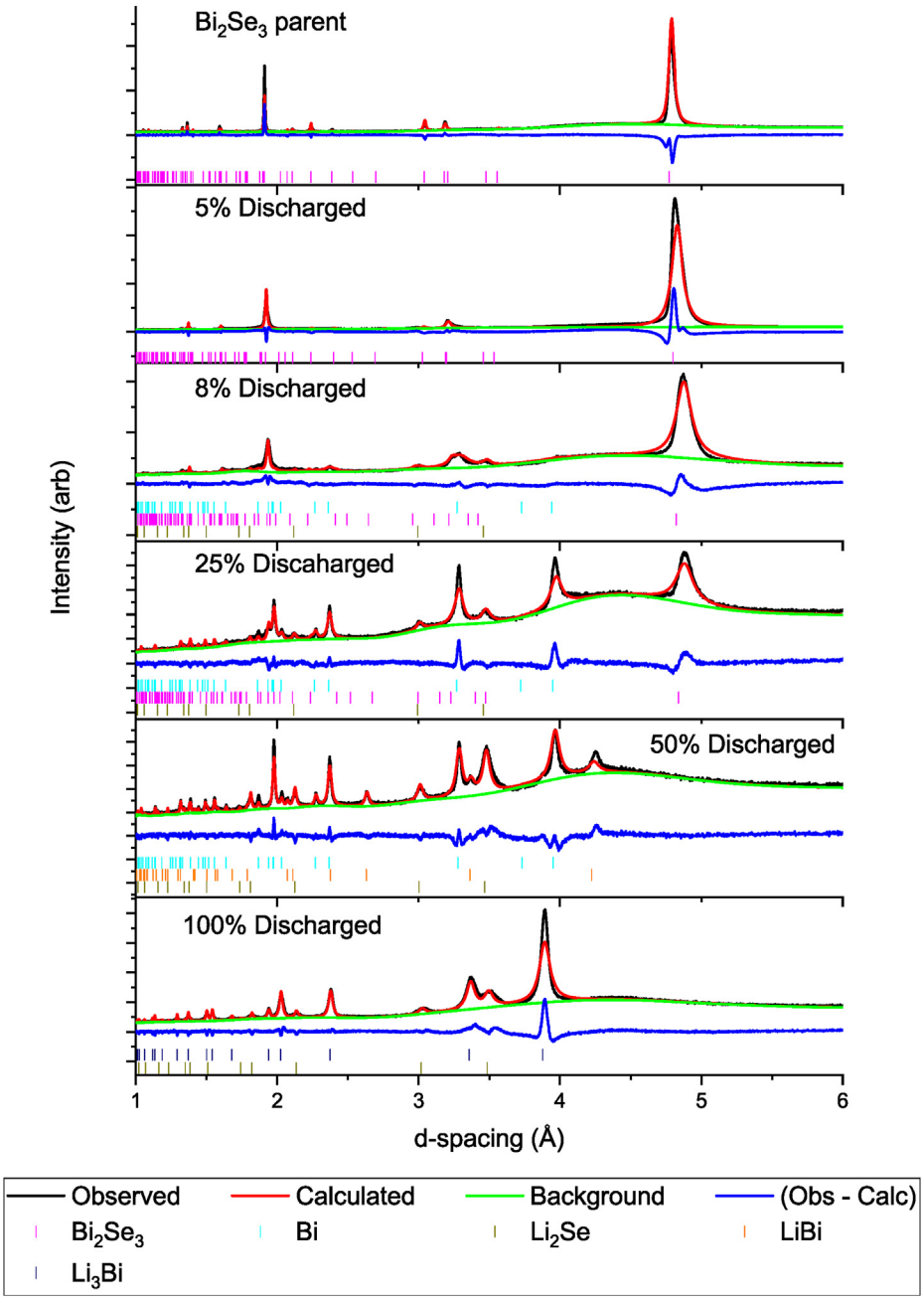

Fig. 5. Rietveld refinements of structural models with PXRD data from Bi_2Se_3 versus Li ex-situ experiments.

were 96, 78 and 42 mAh/g for Li, Na and K half cells respectively. These characteristics indicate that unmodified Bi_2Se_3 is not competitive with existing alkali-ion battery anode materials. Several studies report that the performance of tetradymite-type Sb_2Te_3 in Li and Na ion batteries was significantly enhanced by nano-engineering techniques [7,8,10]. We speculate that such approaches may similarly improve the performance of Bi_2Se_3 in alkali ion batteries, which may affect their competitiveness with graphite. Such investigations are beyond the scope of the current study but are suggested for future works.

The Li and Na systems exhibited at least two plateau-like features in the first discharge profile, which persisted for several subsequent cycles. This suggested that different reactions dominated during these stages of the discharge process. In contrast, the K system had one relatively large plateau, followed by a downward sloping region with some evidence of inflexions. In order to gain further insight into the electrochemical characteristics, differential capacity plots were formulated, and are presented in Fig. 3. The Li and Na systems exhibited two distinct features in the form of troughs, corresponding to the end of each plateau region at 1.6 and 0.75 V, and 1.2 and 0.45 V respectively. The Na system also featured a smaller trough at 0.7 V. The K system showed one sharp trough at 1.1 V, followed by broader or overlapping features at lower voltages, possibly suggesting the occurrence of simultaneous reactions. By the 10^{th} cycle only the Na system exhibited a clear trough, at a potential of 0.4 V. The charging profiles in Li and Na systems exhibited a similar trend with plateau-like features observed in early cycles. The potential onset and capacity of each plateau-like feature differed between systems, and some regions showed multiple steps, e.g., 2–2.5 V in Li and 0.5–0.75 and 1.5–2 V in Na. Differences were noted between all systems, with the K being the most distinct, due to its more sloped character in early cycles. However, all systems exhibited sloped profiles after extended cycling.

Table 2
Lattice parameters and weighted residuals from Rietveld analyses of PXRD data from Bi_2Se_3 versus Li ex-situ experiments.

Sample	Bi_2Se_3 *a* (Å)	Bi_2Se_3 *c* (Å)	Li_2Se *a* (Å)	Li_3Bi *a* (Å)	w*R*
Electrode	4.1382(7)	28.634(1)			13.23%
5%	4.112(5)	28.791(2)			16.00%
8%	3.977(7)	28.925(3)	5.988(3)		8.02%
25%	4.039(1)	29.038(5)	5.987(2)		5.66%
50%			6.0071(7)		5.09%
100%			6.036(1)	6.7152(5)	6.91%

3.3. *Bi_2Se_3 versus Li ex-situ experiments*

Ex-situ PXRD data was collected from Bi_2Se_3 versus Li half cells discharged to the states depicted in Fig. 4. Rietveld analyses were performed on structural models with this data, and the resultant calculated compositions are also shown in Fig. 4. It should be noted that although uncertainties were calculated, error bars are not visible as they are smaller than the datapoint markers. The observed and calculated intensities are shown in Fig. 5, and detailed plots of each refinement are presented in

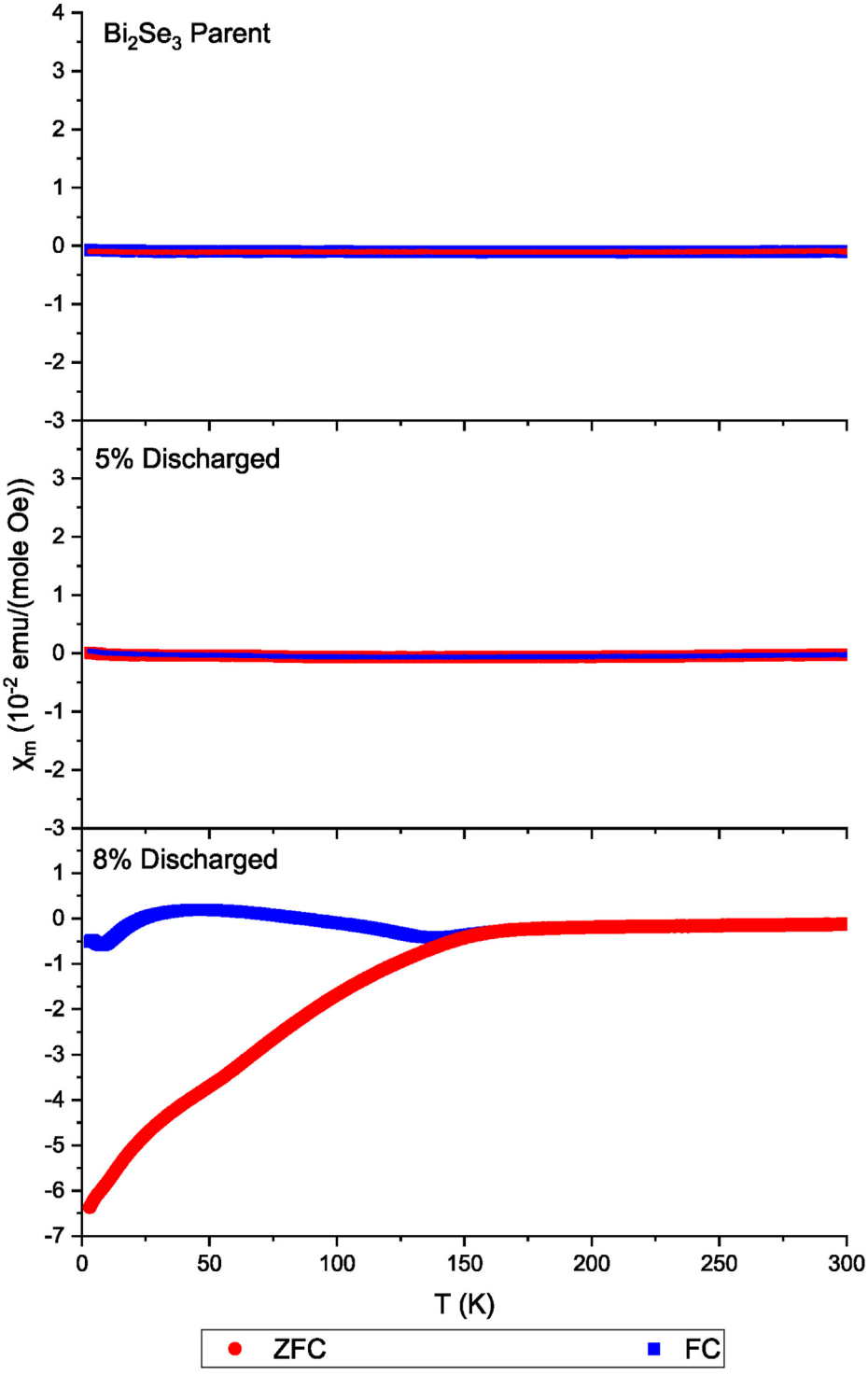

Fig. 6. Magnetic susceptibility of Bi_2Se_3 parent material and Bi_2Se_3 versus Li discharged to 5% and 8%, as a function of temperature, measured in an applied field of 1000 Oe.

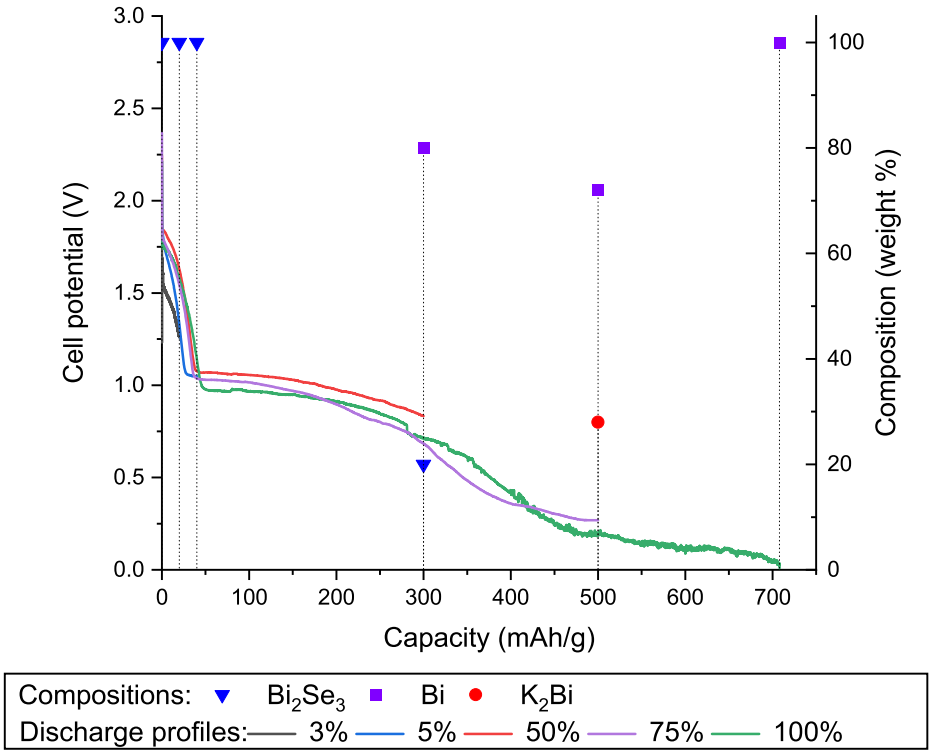

Fig. 7. Discharge profiles and weight fractions for Bi_2Se_3 versus K ex-situ experiments.

Figures SI1-5. Key structural parameters calculated by each refinement are presented in Table 2, and a comprehensive table of parameters is given in the supplementary information (Table SI1).

The 5% discharged sample exhibited no additional reflections compared to the pristine electrode, however the reflections attributable to Bi_2Se_3 were slightly shifted. Rietveld analysis revealed a slight expansion of the *a* and *c* lattice parameters, as shown in Table 2. This result suggested that the initial downward sloped region of the discharge curve corresponded to the intercalation reaction shown in Equation (3).

$$xLi + Bi_2Se_3 \rightarrow Li_xBi_2Se_3 \quad (3)$$

The 8% and 25% discharged samples exhibited additional sets of reflections, which were consistent with Li_2Se and Bi. The reflections attributable to $Li_xBi_2Se_3$ decreased in intensity, and shifted slightly, consistent with further expansion of the *c* lattice parameter. These results suggest that the first plateau region corresponded to the simultaneous occurrence of the intercalation reaction (or completion of intercalation) shown in Equation (3), and the conversion reaction shown in Equation (4).

$$Li_xBi_2Se_3 + (6\text{-}x)Li \rightarrow 3Li_2Se + 2Bi \quad (4)$$

The 50% sample exhibited complete disappearance of the $Li_xBi_2Se_3$ reflections and the appearance of an additional set of reflections consistent with the formation of LiBi. This result suggested that the intermediate sloped region of the discharge profile was associated with the simultaneous occurrence of the conversion reaction shown in Equation (4) and the alloying reaction shown in Equation (5).

$$Bi + Li \rightarrow LiBi \quad (5)$$

The 100% discharged sample exhibited the disappearance of the LiBi reflections, and the appearance of a new set of reflections consistent with the formation of Li_3Bi. This result suggested that the second plateau region corresponded to the alloying reaction shown in Equation (6).

$$LiBi + 2Li \rightarrow Li_3Bi \quad (6)$$

Overall, our results agree with the main conclusions of Ali et al., who concluded that intercalation and conversion reactions occurred during discharge of Bi_2Se_3 versus Li half cells [15]. However, our results represent the first reported XRD-based evidence for these claims. Our finding that alloying reactions occurred in this system had not been previously reported.

As intercalation occurred in the 5% and 8% discharged experiments, magnetic measurements were performed on these samples. Specifically, ZFC and FC experiments were performed on these samples and the parent material, and the results are shown in Fig. 6. Note that the 5% sample appears to be single phase based on the XRD data. The parent material exhibited diamagnetism, which is consistent with previous reports [31]. The 5% likewise exhibited a diamagnetic response, suggesting that the extent of intercalation in this sample did not significantly affect the magnetic properties.

The 8% dataset exhibited diamagnetism above ~150 K, at which point the ZFC and FC curves diverged, indicating that intercalation significantly modified the magnetic properties. It should be noted that the 8% sample contained Bi and Li_2Se in addition to $Li_xBi_2Se_3$, however neither of these materials are likely to be responsible for the observed divergence. This is based on the magnetic properties of these materials, as Bi is known to be strongly diamagnetic [32] and density functional theory calculations suggest that Li_2Se is weakly diamagnetic [33].

3.4. Bi_2Se_3 versus K ex-situ experiments

Bi_2Se_3 versus K ex-situ PXRD experiments were performed at the discharge depths shown in Fig. 7, and the resultant XRD data and Rietveld analyses are shown in Fig. 8. Selected structural parameters calculated by the Rietveld analyses are presented in Table 3. A comprehensive table of parameters (Table SI2) and detailed plots of each refinement (Figures SI6 – 10) are presented in the supplementary information.

The 3 and 5% samples exhibited no additional reflections compared to the parent. The *a* lattice parameter expanded slightly with discharge, and the *c* lattice parameter expanded significantly, suggesting the occurrence of intercalation. This result was consistent with our previous

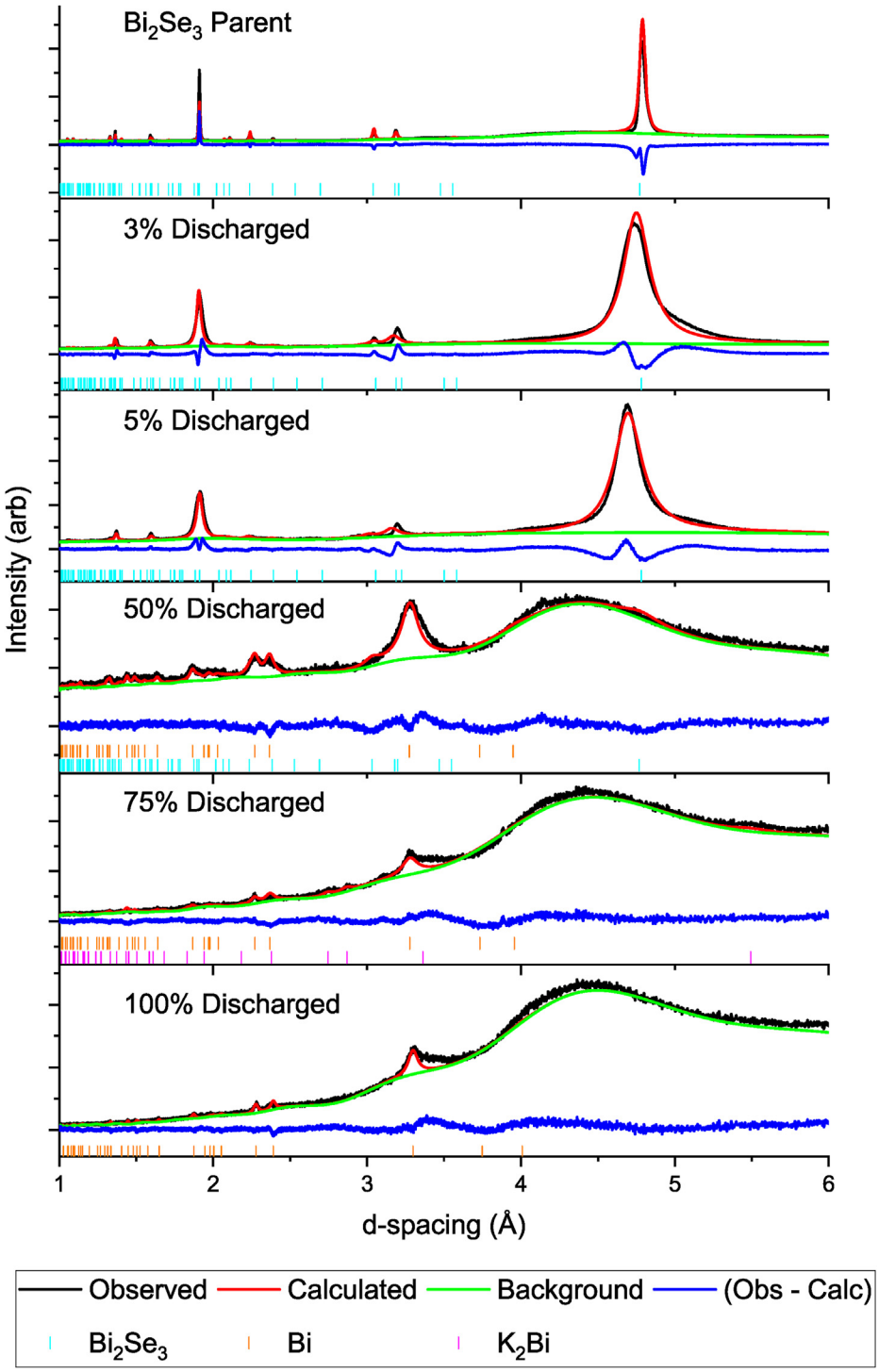

Fig. 8. Rietveld refinements of PXRD data from Bi_2Se_3 versus K ex-situ experiments.

work on the Bi_2Te_3 versus K system, in which a significant degree of intercalation was observed [34].

The 50% sample exhibited a significant decrease in intensity of the reflection set attributable to $K_xBi_2Se_3$, and the appearance of a new set of reflections that were well matched by the Bi structural model. The signal to background ratio significantly decreased, suggesting the formation of an amorphous phase. The increased loss of crystallinity relative to the Li and Na systems may be attributable to the larger ionic radius of K either destabilising the structure or limiting the insertion process. Based on this result we speculate that the first pseudo-plateau region was associated with the conversion reaction shown in Equation (7).

$$Bi_2Se_3 + 6K \rightarrow 3K_2Se + 2Bi \quad (7)$$

The lack of a reflection set consistent with K_2Se may be explained by the evolution of an amorphous form of this phase. This is supported by the observed decrease in signal to background ratio.

The 75% discharged sample exhibited complete disappearance of the Bi_2Se_3 reflections, and the appearance of new reflections consistent with K_2Bi. Additionally, the signal to background ratio further decreased relative to the 50% sample. This result suggested that the intermediate

Table 3
Lattice parameters and weighted residuals from Rietveld analyses of PXRD data from Bi_2Se_3 versus K ex-situ experiments.

Sample	Bi_2Se_3 *a* (Å)	Bi_2Se_3 *c* (Å)	Bi *a* (Å)	Bi *c* (Å)	w*R*
Electrode	4.1382(7)	28.634(1)			13.23%
3%	4.169(6)	28.695(3)			11.23%
5%	4.174(9)	29.014(4)			8.81%
50%			4.535(5)	11.869(7)	4.41%
75%			4.542(6)	11.872(9)	6.58%
100%			4.556(4)	12.025(6)	7.63%

sloped region of the discharge curve was associated with both the conversion reaction shown in Equation (7) and the alloying reaction shown in Equation (8).

$$3Bi + 6K \rightarrow 3K_2Bi \quad (8)$$

The 100% sample exhibited disappearance of the K_2Bi reflections, however no new reflection sets evolved, suggesting the formation of an amorphous phase. Based on the results of our Bi_2Se_3 versus Li experiments, in which Li_3Bi was formed, we speculate that the second plateau was associated with the analogous alloying reaction shown in Equation (9).

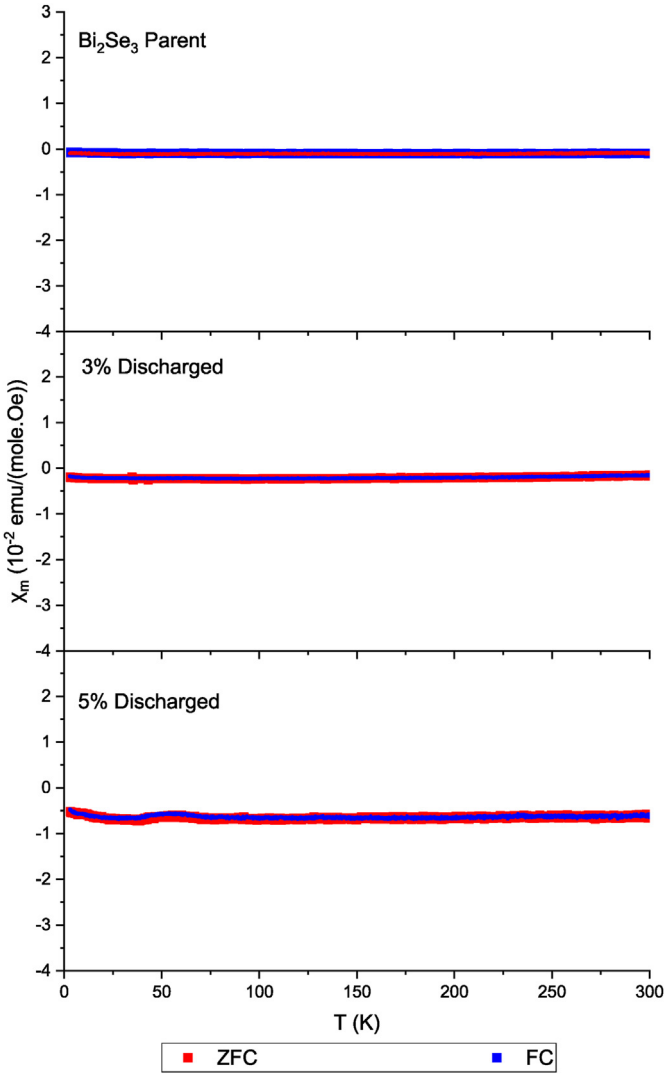

Fig. 9. Magnetic susceptibility of Bi_2Se_3 parent material and Bi_2Se_3 versus K discharged to 3% and 5%, as a function of temperature, measured in an applied field of 1000 Oe.

$$K_2Bi + K \rightarrow K_3Bi \quad (9)$$

We propose that an amorphous or nanosized form of K_3Bi was generated, based on the lack of reflections consistent with this species. However, the persistence of the Bi reflections suggested that this reaction did not proceed to completion.

Magnetic susceptibility experiments were performed on the parent, 3% and 5% samples, and the results are shown in Fig. 9. The 3% and 5% samples exhibited diamagnetism, suggesting that in contrast to Li, intercalation with K did not significantly affect the magnetic properties. Additionally, this result indicates that interlayer spacing was not the primary determinant of magnetic properties for Bi_2Se_3, as the *c* lattice parameter of the 5% K sample exceeded that of the 8% Li sample (29.01 Å vs 28.9 Å). This result is slightly atypical, as many studies have attributed intercalation-induced property modification of layered metal chalcogenides to an increase in interlayer spacing [21]. However such independence is not without precedent, for instance Gamble et al. studied 50 intercalated forms of TaS_2 and found no correlation between interlayer spacing and T_C [35]. Rather, these authors attributed the observed T_C modifications to the intercalant-host charge transfer efficacy [35]. Motivated by this result, we speculate that the difference in ionizability of Li and K may play a role in the interlayer spacing magnetic property independence. Computational methods and further experiments with additional intercalants may elucidate this lack of dependence for Bi_2Se_3, and such investigations are proposed for future works. Although no significant changes in magnetic properties were observed, the 5% sample exhibited minute evidence of a local maximum at 60 K. Resistance versus temperature experiments may clarify whether this represents a magnetic phase transition, and these experiments are suggested for future works.

3.5. *Bi_2Se_3 versus Na ex-situ experiments*

Bi_2Se_3 versus Na ex-situ PXRD experiments were executed at the states shown in Fig. 10, and the corresponding diffractograms and Rietveld analyses are shown in Fig. 11. A table with comprehensive model parameters is provided in the supplementary information (Table SI3) and selected parameters shown in Table 4, as are detailed plots of each refinement (Figures SI11 – 13).

The 3.5% discharged sample showed no additional reflections relative to the parent. Refinement of the Bi_2Se_3 structural model revealed a slight increase in the *c* lattice parameter, and a small decrease in the *a*

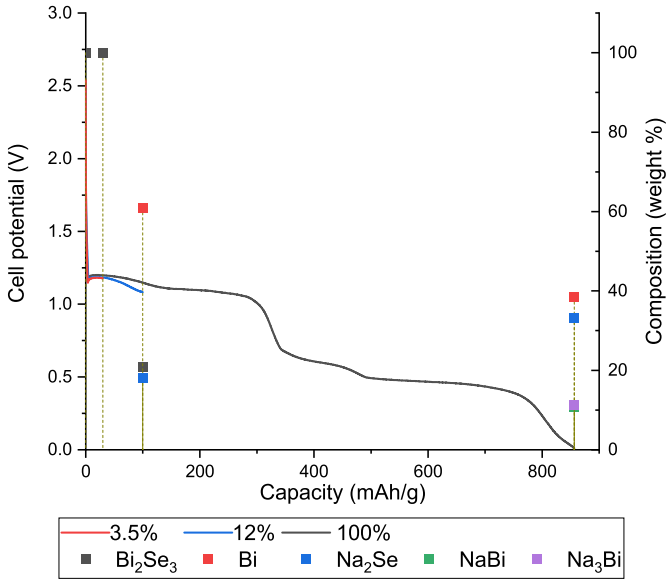

Fig. 10. Discharge profiles and weight fractions for Bi_2Se_3 versus Na ex-situ experiments.

lattice parameter. This result indicated that the initial downward sloped region of the discharge profile corresponded to the intercalation reaction shown in Equation (10). A shoulder was observed in the largest peak, at 6 Å, possibly indicating that this reaction was biphasic.

$$Bi_2Se_3 + Na \rightarrow Na_xBi_2Se_3 \quad (10)$$

The 12% sample exhibited a decrease in intensity of the reflections attributable to $Na_xBi_2Se_3$, and the formation of new sets of reflections consistent with the formation of Bi and Na_2Se. This indicated that the first plateau was dominated by the conversion reaction shown in Equation (11).

$$Na_xBi_2Se_3 + (6\text{-}x)Na \rightarrow 3Na_2Se + 2Bi \quad (11)$$

The 100% discharged sample showed the complete disappearance of the $Na_xBi_2Se_3$ reflections, and the formation of new sets of reflections consistent with the formation of NaBi and Na_3Bi. This indicated that the second plateau region was dominated by the alloying reactions shown in Equation (12) and Equation (13).

$$Bi + Na \rightarrow NaBi \quad (12)$$

$$NaBi + 2Na \rightarrow Na_3Bi \quad (13)$$

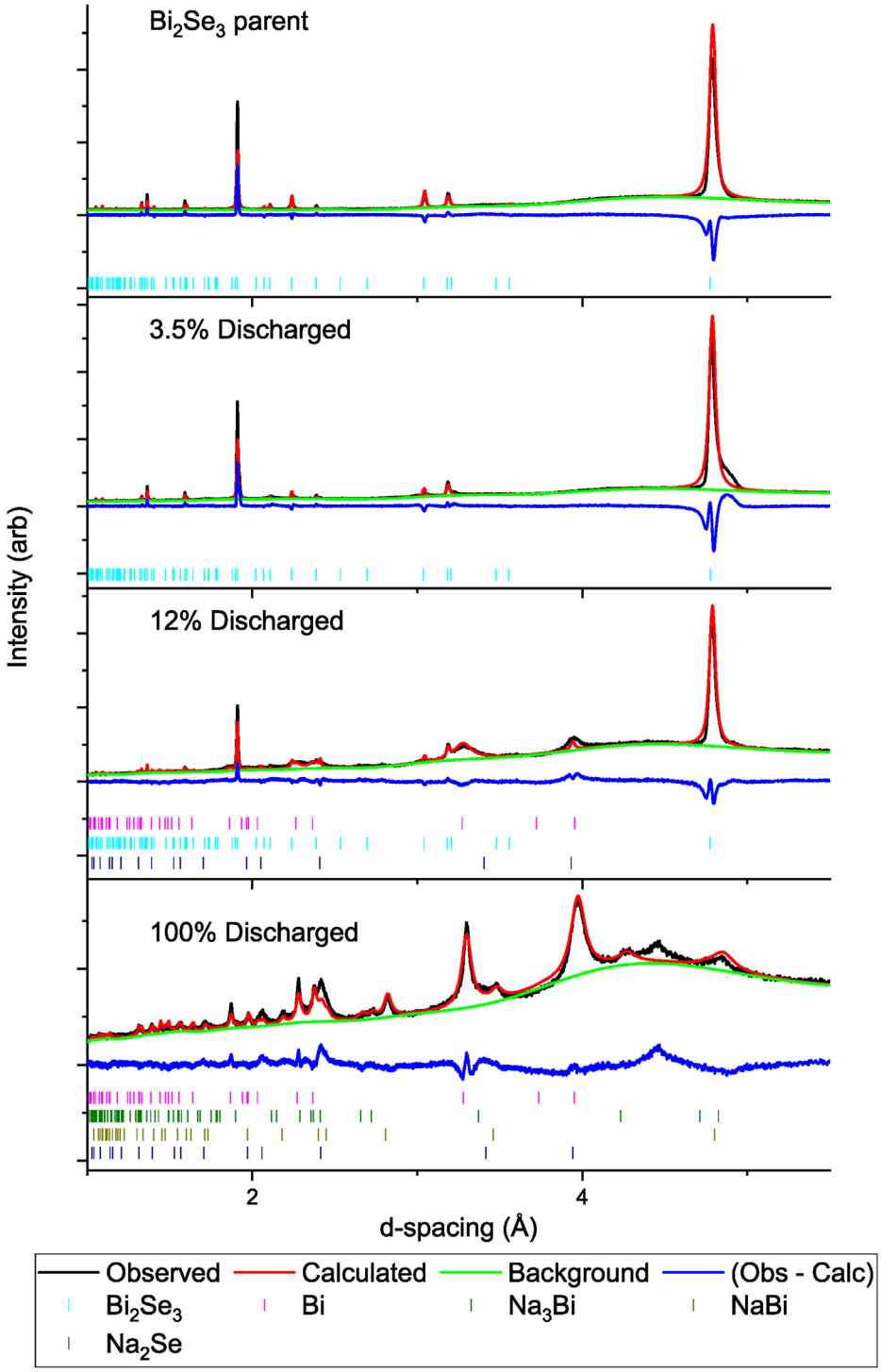

Fig. 11. Rietveld refinements of PXRD data from Bi_2Se_3 versus Na ex-situ experiments.

Table 4
Lattice parameters and weighted residuals from Rietveld analyses of PXRD data from Bi_2Se_3 versus Na ex-situ experiments.

Sample	Bi_2Se_3 *a* (Å)	Bi_2Se_3 *c* (Å)	Bi *a* (Å)	Bi *c* (Å)	w*R*
Electrode	4.1382(7)	28.634(1)			13.23%
3.5%	4.136(1)	28.650(2)			13.23%
12%	4.140(2)	28.637(1)	4.526(3)	11.943(6)	7.75%
100%			4.534(2)	11.880(3)	5.48%

It should be noted that Bi reflections were still present in this sample, suggesting that these alloying reactions did not proceed to completion. Additionally, the signal to background ratio decreased significantly relative to the 12% sample, suggesting the formation of amorphous or nanosized species.

ZFC and FC experiments were performed on the 3.5% discharged sample, and these results are shown in Fig. 12. A slight increase in susceptibility with decreasing temperature was observed at 4 K, but unlike the Li system, no significant alterations of magnetic properties were evident. This may be attributable to the lower extent of intercalation in the Na system, and/or an intercalant ionizability effect. It should be noted that a similar trend was observed in our previous work on tetatradymite-type Sb_2Te_3, in which only Li intercalation induced magnetic property modification [36].

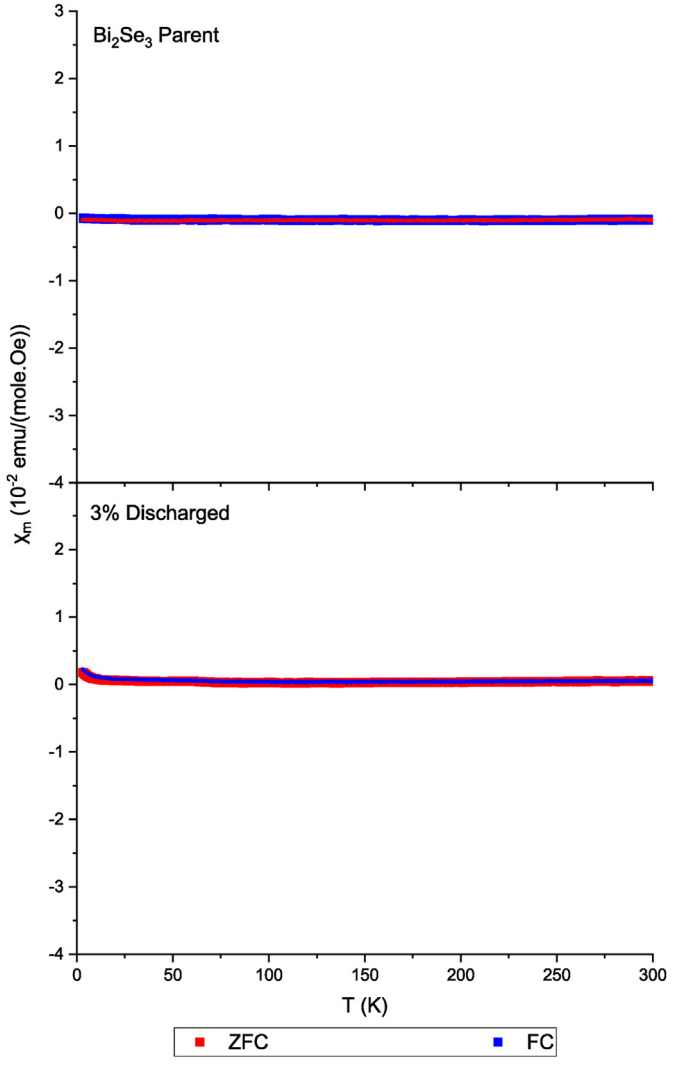

Fig. 12. Magnetic susceptibility of Bi_2Se_3 parent material and Bi_2Se_3 versus Na discharged to 3%, as a function of temperature, measured in an applied field of 1000 Oe.

4. Conclusion

Bi_2Se_3 half cells with Li, Na and K counter-electrodes exhibited high initial discharge capacities 560, 680 and 1000 mAh/g respectively. However, capacity fade was rapid, with 10^{th} cycle capacity decreases of 68%, 79% and 90% respectively. Nano-engineering techniques have been shown to improve cyclability in similar systems, so experiments with these approaches are proposed for future works. Ex-situ PXRD, in conjunction with the observed discharge profiles, indicated that for all systems, the reaction mechanisms involved intercalation, conversion and alloying reactions. The intercalation of Li in the 8% discharged sample induced a bifurcation in the ZFC and FC curves below ~150 K. In contrast, Na and K intercalation did not significantly affect the magnetic properties of the resultant single-phase products. These results suggest that interlayer spacing was not the primary determinant of magnetic properties, and intercalant ionizability may play a role. This trend was consistent with our previous work on tetradymite-type Sb_2Te_3. Future works involving computational methods and intercalation of other species are proposed, to further investigate this relationship.

CRediT authorship contribution statement

Conrad Gillard: Investigation, data analysis and writing. **Kathleen Djohari:** Investigation. **Partha Pratim Jana:** Methodology, Conceptualization. **Maxim Avdeev:** Investigation, Methodology, Resources. **Neeraj Sharma:** Conceptualization, data analysis and writing, All authors contributed to various aspects of the presented research.

Declaration of competing interest

The authors declare that they have no known competing financial interests or personal relationships that could have appeared to influence the work reported in this paper.

Acknowledgement

Conrad Gillard was supported by an Australian Government Research Training Program (RTP) Scholarship. Conrad Gillard would also like to thank AINSE Limited for providing financial assistance (Award - PGRA). This work was financially supported by the Australian Research Council Discovery programs (DP200100959 and FT200100707).

Appendix A. Supplementary data

Supplementary data to this article can be found online at https://doi.org/10.1016/j.jssc.2021.122241.

References

[1] Z. Tian, S. Lee, G. Chen, Comprehensive review of heat transfer in thermoelectric materials and devices, Ann. Rev. Heat Transfer, 17 (2014).
[2] H. Zhang, et al., Topological insulators in Bi 2 Se 3, Bi 2 Te 3 and Sb 2 Te 3 with a single Dirac cone on the surface, Nat. Phys. 5 (6) (2009) 438.
[3] M.-X. Wang, et al., The coexistence of superconductivity and topological order in the Bi2Se3 thin films, Science 336 (6077) (2012) 52–55.
[4] D.L. Medlin, G. Snyder, Atomic-scale interfacial structure in rock salt and tetradymite chalcogenide thermoelectric materials, JOM (J. Occup. Med.) 65 (3) (2013) 390–400.
[5] Z. Ding, et al., Lithium intercalation and exfoliation of layered bismuth selenide and bismuth telluride, J. Mater. Chem. 19 (17) (2009) 2588–2592.
[6] J. Bludska, et al., Lithium ions in the van der Waals gap of Bi2Se3 single crystals, J. Solid State Chem. 183 (12) (2010) 2813–2817.
[7] Z. Yang, et al., Facile synthesis and in situ transmission electron microscopy investigation of a highly stable Sb2Te3/C nanocomposite for sodium-ion batteries, Energy Storage Mater. 9 (2017) 214–220.
[8] K.-H. Nam, J.-H. Choi, C.-M. Park, Highly reversible Na-ion reaction in nanostructured Sb2Te3-C composites as Na-ion battery anodes, J. Electrochem. Soc. 164 (9) (2017) A2056–A2064.
[9] X. Zhao, et al., Electrochemical properties of some Sb or Te based alloys for candidate anode materials of lithium-ion batteries, J. Alloys Compd. 315 (1–2) (2001) 265–269.

[10] K.-H. Nam, C.-M. Park, Layered Sb 2 Te 3 and its nanocomposite: a new and outstanding electrode material for superior rechargeable Li-ion batteries, J. Mater. Chem. 4 (22) (2016) 8562–8565.
[11] R. Liu, et al., Enhanced thermoelectric performance of Te-doped Bi2Se3− xTex bulks by self-propagating high-temperature synthesis, Crystals 7 (9) (2017) 257.
[12] J. Chen, et al., Direct tuning of electrical properties in nano-structured Bi 2 Se 0.3 Te 2.7 by reversible electrochemical lithium reactions, Chem. Commun. 47 (44) (2011) 12173–12175.
[13] J. Chen, et al., Top-down fabrication of nano-scaled Bi2Se0. 3Te2. 7 associated by electrochemical Li intercalation, Dalton Trans. 40 (2) (2010) 340–343.
[14] Z. Lijuan, et al., Study on the insertion behaviors of lithium-ions into Bi_2 Te_3/ Polyaniline composites electrodes [J] 4, Rare Metal Materials and Engineering, 2005.
[15] Z. Ali, et al., Effect of synthesis technique on electrochemical performance of bismuth selenide, J. Power Sources 229 (2013) 216–222.
[16] Y.S. Hor, et al., Superconductivity in Cu x Bi 2 Se 3 and its implications for pairing in the undoped topological insulator, Phys. Rev. Lett. 104 (5) (2010), 057001.
[17] J. Bludská, et al., Lithium intercalation into the tetradymite-type selenides Bi2-xInxSe3, Phil. Mag. B 76 (6) (1997) 867–873.
[18] G. Han, et al., In-doped Bi 2 Se 3 hierarchical nanostructures as anode materials for Li-ion batteries, J. Mater. Chem. 2 (19) (2014) 7109–7116.
[19] R. Jin, et al., Hierarchical Bi 2 Se 3–x S x microarchitectures assembled from ultrathin polycrystalline nanosheets: solvothermal synthesis and good electrochemical performance, J. Mater. Chem. 1 (36) (2013) 10942–10950.
[20] F. Mao, et al., Solvothermal synthesis and electrochemical properties of S-doped Bi 2 Se 3 hierarchical microstructure assembled by stacked nanosheets, RSC Adv. 6 (44) (2016) 38228–38232.
[21] Y. Jung, Y. Zhou, J.J. Cha, Intercalation in two-dimensional transition metal chalcogenides, Inorg. Chem. Front. 3 (4) (2016) 452–463.
[22] Z. Guo, F. Sun, W. Yuan, Chemical intercalations in layered transition metal chalcogenides: syntheses, structures, and related properties, Cryst. Growth Des. 17 (4) (2017) 2238–2253.
[23] T. Marks, et al., A guide to Li-ion coin-cell electrode making for academic researchers, J. Electrochem. Soc. 158 (1) (2011) A51–A57.
[24] B.H. Toby, R.B. Von Dreele, GSAS-II: the genesis of a modern open-source all purpose crystallography software package, J. Appl. Crystallogr. 46 (2) (2013) 544–549.
[25] Y. Liu, B.V. Merinov, W.A. Goddard, Origin of low sodium capacity in graphite and generally weak substrate binding of Na and Mg among alkali and alkaline earth metals, Proc. Natl. Acad. Sci. Unit. States Am. 113 (14) (2016) 3735–3739.
[26] Sigma-Aldrich, Graphite anode powder [cited 2020 19 April]; Available from: https://www.sigmaaldrich.com/catalog/product/aldrich/907154?lang=en&region=AU.
[27] Sigma-Aldrich, *Bismuth(III) selenide* [cited 2021 12 January]; Available from: https://www.sigmaaldrich.com/catalog/product/aldrich/401080?lang=en&region=AU.
[28] Y. Wen, et al., Expanded graphite as superior anode for sodium-ion batteries, Nat. Commun. 5 (1) (2014) 1–10.
[29] L. Fan, et al., Graphite anode for a potassium-ion battery with unprecedented performance, Angew. Chem. Int. Ed. 58 (31) (2019) 10500–10505.
[30] Y.-P. Wu, E. Rahm, R. Holze, Carbon anode materials for lithium ion batteries, J. Power Sources 114 (2) (2003) 228–236.
[31] B. Irfan, R. Chatterjee, Magneto-transport and Kondo effect in cobalt doped Bi2Se3 topological insulators, Appl. Phys. Lett. 107 (17) (2015) 173108.
[32] Y. Fuseya, M. Ogata, H. Fukuyama, Transport properties and diamagnetism of Dirac electrons in bismuth, J. Phys. Soc. Jpn. 84 (1) (2015), 012001.
[33] K. Persson, Materials data on Li2Se (SG:225) by materials project, 2014 [cited 2021 25/1/2021]; Available from: https://materialsproject.org/materials/mp-2286/.
[34] C.H. Gillard, et al., Electrochemical phase evolution of tetradymite-type Bi2Te3 in lithium, sodium and potassium ion half cells, J. Alloys Compd. (2020) 155621.
[35] F. Gamble, et al., Superconductivity in layered structure organometallic crystals, Science 168 (3931) (1970) 568–570.